Wavelength-Dependent Change of Retinal Nerve Fiber Layer Reflectance in Glaucomatous Retinas

Xiang-Run Huang,[1,2] *Ye Zhou,*[2] *Robert W. Knighton,*[1] *Wei Kong,*[1] *and William J. Feuer*[1]

Purpose. Retinal nerve fiber layer (RNFL) reflectance is often used in optical methods for RNFL assessment in clinical diagnosis of glaucoma, yet little is known about the reflectance property of the RNFL under the development of glaucoma. This study measured the changes in RNFL reflectance spectra that occurred in retinal nerve fiber bundles with different degrees of glaucomatous damage.

Methods. A rat model of glaucoma with laser photocoagulation of trabecular meshwork was used. Reflectance of the RNFL in an isolated retina was measured at wavelengths of 400–830 nm. Cytostructural distribution of the bundles measured optically was evaluated by confocal imaging of immunohistochemistry staining of cytoskeletal components, F-actin, microtubules, and neurofilaments. RNFL reflectance spectra were studied in bundles with normal-looking appearance, early F-actin distortion, and apparent damage of all cytoskeletal components. Changes of RNFL reflectance spectra were studied at different radii (0.22, 0.33, and 0.44 mm) from the optic nerve head (ONH).

Results. Bundles in 30 control retinas and 41 glaucomatous retinas were examined. In normal retinas, reflectance spectra were similar along the same bundles. In glaucomatous retinas, reflectance spectra changed along bundles with the spectra becoming flatter as bundle areas approached the ONH.

Conclusions. Elevation of intraocular pressure (IOP) causes nonuniform changes in RNFL reflectance across wavelengths. Changes of reflectance spectra occur early in bundles near the ONH and prior to apparent cytoskeletal distortion. Using the ratio of RNFL reflectance measured at different wavelengths can provide early and sensitive detection of glaucomatous damage. (*Invest Ophthalmol Vis Sci.* 2012;53:5869–5876) DOI: 10.1167/iovs.12-10001

Glaucoma causes damage of the retinal nerve fiber layer (RNFL), which consists of axons of retinal ganglion cells. In clinical diagnosis of glaucoma, red-free fundus photography can often identify RNFL defects years before detectable visual loss.[1–3] Currently often-used optical coherence tomography (OCT) provides quantitative measurement of RNFL thickness and has high sensitivity and specificity to identify glaucoma patients with moderate to severe RNFL damage.[4–7] However, studies have shown that OCT is unable to detect some subtle RNFL defects that are apparent in red-free photographs and, overall, OCT is not better than fundus photography assessed by experienced observers in distinguishing normal eyes from those with early glaucomatous damage, especially when it appears as localized defects.[8–13] Reasons for high resolution OCT being not superior in detecting RNFL defects may include limited lateral resolution, algorithm limitations for detecting RNFL defects, and large variation of RNFL thickness in normative databases.[6,9–11] In this study, we proposed the additional hypothesis that changes of RNFL reflectance due to glaucomatous damage are not uniform across wavelengths.

RNFL reflectance arises from light scattering by cylindrical structures of axons.[14,15] In normal retina, RNFL reflectance is wavelength dependent with reflectance high at visible wavelengths and lower at near infrared wavelengths.[15] An RNFL reflectance spectrum can be described by a two-mechanism scattering model, in which both thin and thick cylinders contribute to the reflectance, with thin cylinders contributing more at short wavelengths and thick cylinders dominating the reflectance at long wavelengths.[15] Studies show that microtubules (MTs) contribute to RNFL reflectance; other scattering structures have not yet been identified.[16,17]

Glaucoma damages axonal cytostructure, including F-actin, MTs, and neurofilaments (NFs).[18–26] Degree of damage varies from early distortion of F-actin to severe distortion and total loss of the axonal cytoskeleton. Early cytostructural distortion occurs prior to thinning of the RNFL.[25,26] Recent studies show that a decrease in RNFL reflectance also precedes changes in RNFL thickness (Vermeer KA, et al. *IOVS* 2011;52:ARVO E-Abstract 3666)[27,28] and, therefore, direct measurement of RNFL reflectance may provide detection of axonal damage at a time during which damage is reversible.

Because each cytostructural component responds differently to glaucomatous damage, RNFL reflectance is expected to have nonuniform change across wavelengths. In this study, we used a rat model of glaucoma to study wavelength dependence of RNFL reflectance in retinas with different degrees of glaucomatous damage.

Materials and Methods

Rat Model of Glaucoma

Female Wistar rats weighing 250–350 g were used in this study. The rat model of glaucoma has been described in detail previously.[25] Briefly, animals were anesthetized with intraperitoneal ketamine (50 mg/kg) and xylazine (5 mg/kg) and topical proparacaine 1% eye drops. Experimental glaucoma was induced by translimbal laser photocoagulation of the trabecular meshwork.[29] The laser treatment (a diode laser with a wavelength of 532 nm, 500-mW power, 0.6-second duration, 50-μm–diameter spot size) was administered in the left eye of each rat. Around

From the [1]Bascom Palmer Eye Institute and the [2]Department of Biomedical Engineering, University of Miami, Miami, Florida.

Supported by National Institutes of Health Grant R01-EY019084, American Health Assistance Foundation Grant G2008-033, National Institutes of Health Core Grant P30-EY014801, a Department of Defense Career Development Award, and an unrestricted grant from Research to Prevent Blindness.

Submitted for publication April 10, 2012; revised June 25 and July 19, 2012; accepted July 23, 2012.

Disclosure: **X.-R. Huang**, None; **Y. Zhou**, None; **R.W. Knighton**, None; **W. Kong**, None; **W.J. Feuer**, None

Corresponding author: Xiang-Run Huang, Bascom Palmer Eye Institute, University of Miami Miller School of Medicine, 1638 NW Tenth Avenue, Miami, FL 33136; xhuang3@med.miami.edu.

55 to 60 trabecular burns were evenly distributed. A second treatment after a week was applied to those eyes that did not maintain elevated IOP. The contralateral eye was untreated and served as the control.

A rebound tonometer (Tonolab; Colonial Medical Supply, Franconia, NH) was used to monitor the IOP after the animals were anesthetized. The IOP in both eyes was measured just before treatment and 1, 3, 5, and 7 days after treatment and then once a week until enucleation or the IOP returned to its baseline value. For each rat, graphs of IOP (IOP in mm Hg versus days after treatment) for treated and fellow eyes were constructed. Cumulative IOP, the area between the curves for the two eyes in units of mm Hg-days, was calculated.

All experiments adhered to the ARVO Statement for the Use of Animals in Ophthalmic and Vision Research. The protocol for the use of animals was approved by the Animal Care and Use Committee of the University of Miami.

Tissue Preparation and RNFL Reflectance Measurement

Animals were sacrificed for optical experiments at approximately 3 weeks after the first laser treatment. Both eyes of each animal were used in the study. Retinas were isolated free from the pigment epithelium and choroid. Tissue preparation, following previously developed procedures,[27,30] was carried out with intense white illumination, which thoroughly bleached the visual pigment in the photoreceptors and ensured that the reflectance in this layer remained constant. A prepared retina was placed in a chamber perfused with warm physiologic solution to maintain the tissue alive.

A multispectral imaging microreflectometer was used to detect RNFL reflectance. The device has been described in detail previously.[30] Images of the RNFL were collected by a cooled charge-coupled device (CCD camera, U47+ Digital Imaging System; Apogee Instruments Inc., Roseville, CA) at wavelengths ranging from 400 nm to 830 nm. In an experiment, nerve fiber bundles were measured at near maximum reflectance. Black images, taken with the same exposure duration but with the light source off, were subtracted from each image to compensate for the dark current and bias level of the CCD. The resulting pixel values were directly proportional to reflected intensity. To calculate relative reflectance of the RNFL, images were also taken of a diffuse white reflector (Kodak 6080 White Reflectance Coating; Eastman Kodak Company, Rochester, NY). Pixel values of retinal images were then converted to relative reflectance $\boldsymbol{R_\lambda}$ by

$$R_\lambda = \gamma_\lambda \frac{P}{P_w}\frac{T_w}{T} \quad (1)$$

where γ_λ is a known reflectance coefficient of the white reflector at wavelength λ; P and P_w are pixel values of the tissue and white reflector, respectively; and T and T_w are their corresponding exposure durations. Hereafter, the relative reflectance is simply called reflectance. To compensate possible tissue shift during measurements, an entire set of images was registered by horizontal and vertical translation.

Calculation of RNFL Reflectance and Comparison of Spectral Pattern

To calculate RNFL reflectance, bundle areas were selected at distances of approximately 0.22 mm, 0.33 mm, and 0.44 mm (r_a, r_b, and r_c) from the center of the ONH. Reflectance measured on bundle areas included light reflected from the RNFL and its underlying tissue. It is anatomically reasonable to assume that the tissue underlying the RNFL is similar to the tissue between bundles, that is, the gaps seen in Figure 1. Because the weak scattering of the RNFL caused little attenuation to an incident beam, we assumed that the reflectance from deep layers was approximately the same as that from nearby gap areas between bundles. Areas, therefore, were chosen both on bundles and on nearby gaps between bundles and the average reflectance of gap areas was then subtracted from the total reflectance measured on the bundle areas to get an estimate of the bundle reflectance alone (Fig. 1).[27,30]

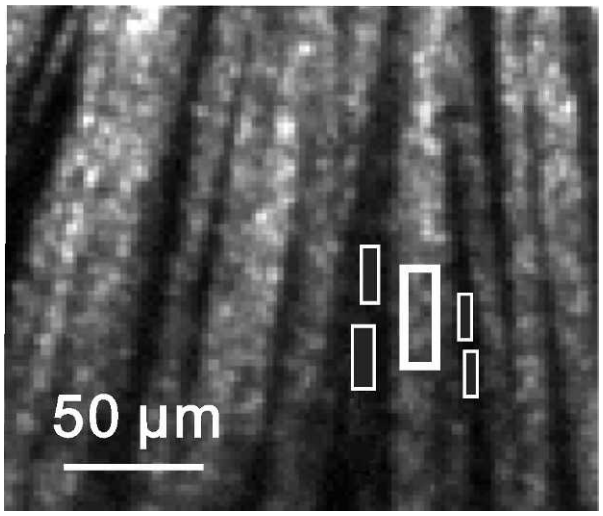

Figure 1. Calculation of RNFL reflectance. Nerve fiber bundles appear as bright stripes and are separated by gaps—the darker space between bundles. The reflectance (R) of the defined bundle area (*thick box*) includes the reflectance of the bundle alone (R_{bundle}) and its underlying tissue ($R_{background}$). The reflectance of the bundle alone is calculated as $R_{bundle} = R - R_{background}$, where $R_{background}$ is estimated from the average reflectance of nearby gap areas (*thin boxes*). Image at 440 nm.

RNFL reflectance and its spectral pattern depend on measurement geometry. A detailed description of the scattering geometry can be found in an earlier publication.[15] RNFL reflectance was calculated for those bundles that were measured at on-peak or near-peak reflectance. The incident and scattering angles for bundle areas to be analyzed were also calculated. Only those bundle areas with incident and scattering angles varying $\pm$ 10° and $\pm$15°, respectively, around their mean values were used for data comparison. Because RNFL reflectance depends on wavelength, mean reflectance at wavelengths of 400 to 440 nm ($R_{400-440}$); 500 to 560 nm ($R_{500-560}$); and 740 to 830 nm ($R_{740-830}$) were calculated respectively. To compare patterns of reflectance spectra, each spectrum was normalized to its $R_{500-560}$. Reflectance ratios, calculated as relative reflectance at short and long wavelengths $\rho_S = R_{400-440} / R_{500-560}$ and $\rho_L = R_{740-830} / R_{500-560}$, respectively, were then used to quantitatively compare changes of reflectance spectra.

For each retina, two to three bundles were analyzed. Bundles from the same retina were separated by at least one major blood vessel to avoid repeat sampling of similar bundles in one retina.

Two-Mechanism Scattering Modeling of RNFL Reflectance Spectrum

RNFL reflectance arises from light scattering by cylindrical structures of the RNFL. In normal rat retina, an RNFL reflectance spectrum can be described by a two-mechanism scattering model.[15] The modeling demonstrates that both thin and thick cylindrical structures may contribute to RNFL reflectance. In the model, the thick cylinders have a "triangle" distribution with no radii below a certain value s and the proportion of cylinders at each radius declining linearly from s to zero over a range w (see the *inset* in Fig. 4). The thin cylinders could have any radius (r_t) that is much less than the shortest wavelength. By assuming refractive indexes for the cylinders, the shape of the RNFL reflectance spectrum can be characterized by three parameters (s, w, n), with n being the

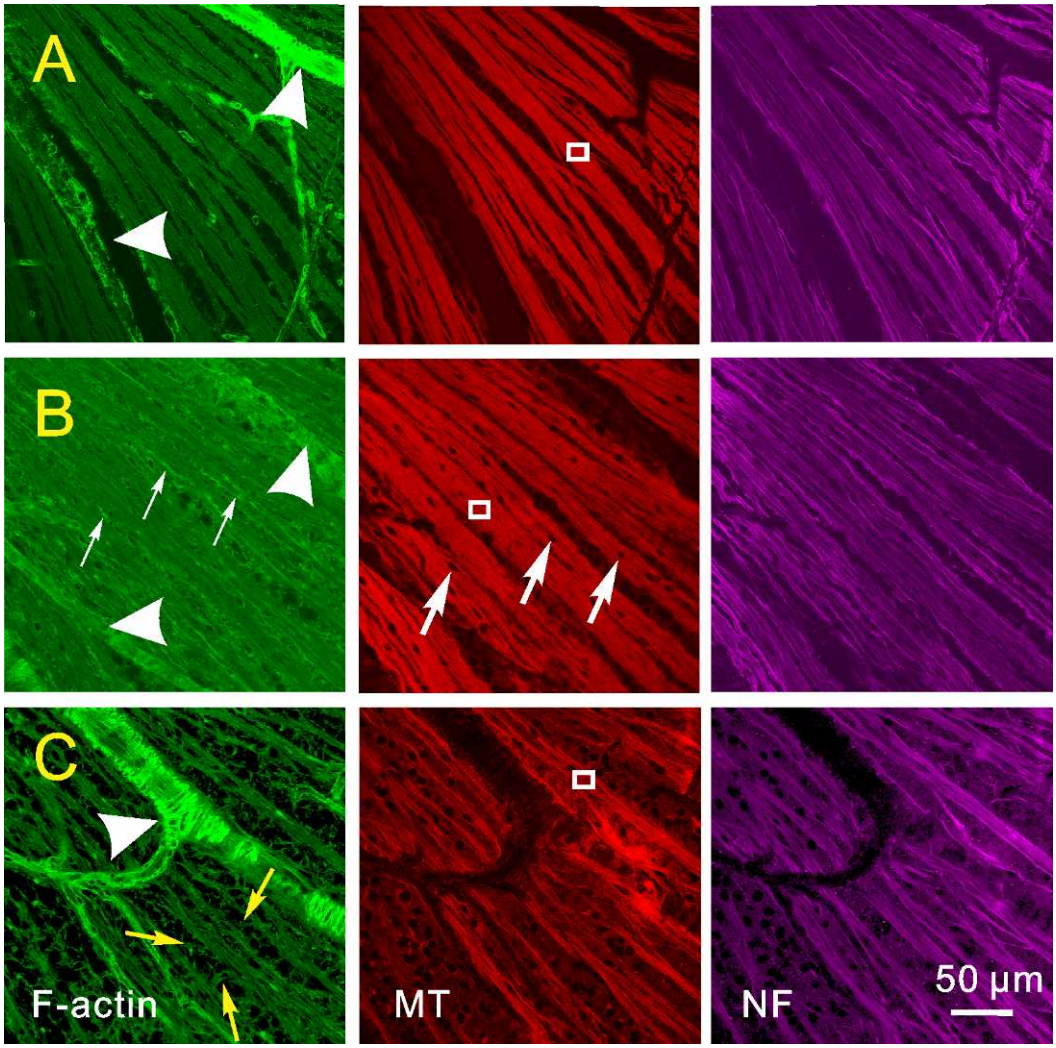

Figure 2. Axonal cytoskeleton in retinas with different degrees of glaucomatous damage. Retinas were stained simultaneously for F-actin, MTs, and NFs. (**A**) Normal-looking bundles with uniformly stained cytoskeletal components within the bundles. (**B**) Bundles with irregularly stained F-actin (*thin white arrows*) and nuclei (*thick white arrows*) embedded within the bundles. (**C**) Severely damaged bundles with apparent network (*yellow arrows*) of F-actin between bundles and distorted strands of F-actin, MTs, and NFs within bundles. Images taken with 40× oil objective. *Arrow heads*: blood vessels.

number of thin cylinders per unit-thick cylinder mechanism. We assigned a value of 10 nm, the equivalent radius of microtubules, and a relative refractive index (m_t) of 1.08 to the thin cylinders and an arbitrary refractive index (m_T) of 1.03 to the thick cylinders.[15] By using a normalized reflectance spectrum, fitted values of s and w are independent of the assigned r_t, m_t, and m_T.[31] However, n depends on these assigned values.

In this study, we used the two-mechanism scattering model to fit measured RNFL reflectance spectra in the control and treated retinas by assuming that m_t and m_T did not change with glaucomatous damage. The fitted parameters (s, w, n) then may provide insight into relative contributions of different structural mechanisms to the RNFL reflectance under the development of glaucoma.

All data analysis was implemented with customized software programmed in a numerical computing environment (MATLAB; The MathWorks, Inc., Natick, MA).

Evaluation of Axonal Cytoskeleton

After reflectance measurement, retinas were fixed and processed for immunohistologic evaluation of axonal cytoskeleton. The preparation details of the immunohistologic staining and confocal microscopic imaging have been published previously.[25] Briefly, retinas were stained with antineurofilament antibody to label NFs (a primary antibody of 1:500 rabbit antineurofilament 200 kD, Sigma; a secondary antibody of 1:250 Alex Fluor 647 goat antirabbit IgG; Invitrogen, Grand Island, NY); anti-β-tubulin antibody to stain MTs (1:100 Cy3 conjugated anti-β-tubulin antibody; Sigma); and a solution of phalloidin to identify F-actin (1:100 Alexa Fluor 488 Phalloidin; Invitrogen). The antineurofilament antibody is a polyclonal antibody that has cross-reactivity against both phosphorylated and nonphosphorylated forms. In addition, nuclei were identified by 4′,6-diamidino-2-phenylindole (DAPI) fluorescent counterstain. Confocal imaging with a 40× oil objective provided both en face and cross-sectional images of retinas covering a 1.2 × 1.2-mm area around the ONH with a pixel resolution of 0.75 μm.

To relate axonal cytostructure to its measured reflectance, the location of an individual nerve fiber bundle measured optically was identified in the corresponding confocal and optical images of the same retina by matching the blood vessel patterns.[27,32] In glaucomatous retina, the appearance of bundles was graded as normal appearance

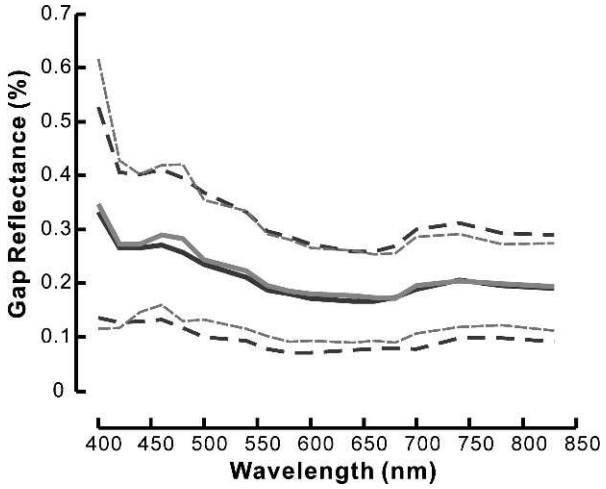

Figure 3. Reflectance spectra of gap areas are similar in normal (*black line*) and glaucomatous (*gray line*) retinas. *Solid lines*: average spectra of all gap areas defined for the bundles analyzed in this study. *Dashed lines*: ± standard deviation. Reflectance value was calibrated with the diffuse white reflector (see text for details).

(G1), distortion of F-actin (G2), and distortion of all cytoskeletal components (G3).

Statistical Analysis

Reflectance ratios, ρ_S and ρ_L, between normal and treated groups were compared with a linear mixed-model analysis accounting for the correlation between multiple measurements made on the same retina and post hoc least-significant difference tests. Incident angle and scattering angles were compared using an unequal variance *t*-test. The influence of treatment group and bundle location on ρ_S, ρ_L, and fitted parameters (*s*, *w*, *n*) was studied with the analysis of covariance formulation of the general linear model, which included tests of group interactions (SPSS/PASW Statistics 18; IBM Corporation, Somers, NY). The significance level was set at $P < 0.05$.

Averaged parameters are reported as mean ± standard deviation. The fitted parameters (*s, w, n*) are reported as fitted value ± standard error with the standard error estimated from the Jacobian matrix of the nonlinear least square fitting of RNFL reflectance spectra.[33]

Results

Forty-one Wistar rats were treated unilaterally. The mean IOP increased from 11 ± 0.5 to 41 ± 8 mm Hg. The cumulative IOP ranged from 87 to 311 mm Hg days with the mean of 152 ± 61 mm Hg days. Fifty-two bundles of 30 control retinas (OD) and 131 bundles of 41 treated retinas (OS) were examined. All bundles satisfied the selection criteria described above. The average incident angles were 16° ± 7° for both control and treated retinas; and the average scattering angles were 161° ± 11° and 162° ± 12° for control and treated retinas, respectively.

Change of Axonal Cytoskeleton in Glaucomatous Retinas

Nerve fiber bundles were identified as bright stripes in en face images by fluorescence-labeled F-actin, MTs, and NFs. In the control retinas, the stain of the cytoskeletal components appeared strong and uniform within bundles.

IOP elevation caused localized distortion of axonal cytoskeleton. Normal-looking bundles and bundles with different degrees of cytoskeletal distortion were often found in the same retinas. Figure 2A shows a retinal region with normal-looking bundles (G1), which have approximately uniform, stained cytoskeletons within the bundles and well-defined bundle boundaries. At an early stage of glaucomatous damage (G2), stains of MTs and NFs were nearly normal-looking; however, nuclei were embedded in the RNFL and the en face image of F-actin showed strings with bright phalloidin stains and indiscernible bundle boundaries (Fig. 2B). In further damaged retinas (G3), strings of F-actin, MTs, and NFs became apparent within bundles; stains of all three components were not uniform along bundles; and an F-actin network, appearing as phalloidin stain, was apparent between bundles (Fig. 2C). Detailed studies of the cytoskeletal change have been published separately.[21,25] In this study, confocal images were

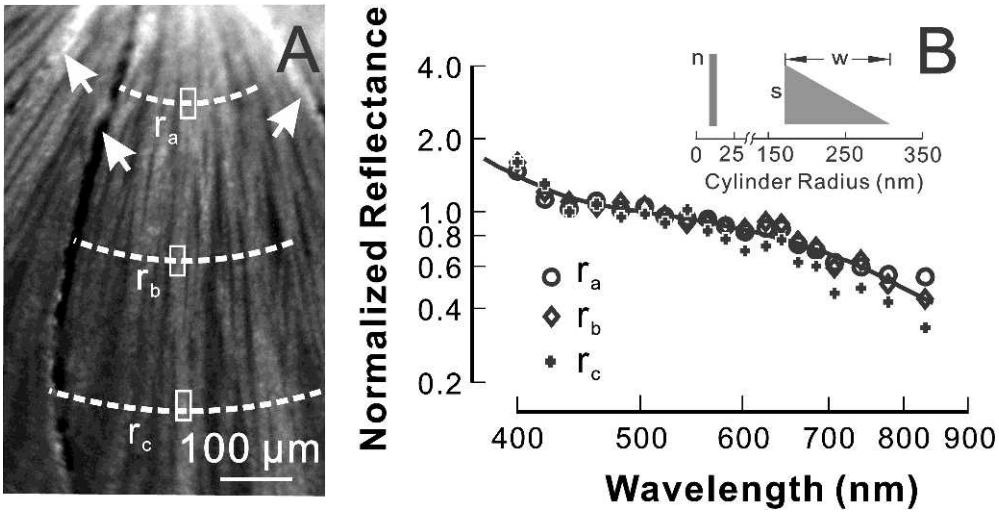

Figure 4. RNFL reflectance spectra in a normal retina. (**A**) Reflectance image (440 nm) shows bundles as bright stripes against a darker background. Reflectance of bundle areas (*box*) was analyzed at radii of 0.22 (r_a), 0.33 (r_b), and 0.44 (r_c) mm from the center of the ONH (not shown). *Arrow*: blood vessel. (**B**) The RNFL reflectance spectra of the bundle areas defined in **4A**. The reflectance decreases with increasing wavelength. The reflectance spectra are similar along the same bundle. *Solid line*: fitted spectrum with a two-mechanism scattering model with parameters $n = 134 \pm 38$, $s = 165 \pm 14$ nm, $w = 141 \pm 47$ nm, and $R^2 = 0.97$. The *inset* shows the scattering model (see text for details).

Table 1. RNFL Reflectance Ratios of the Control Retinas at Different Radii

	$r_a = 0.22$ mm	$r_b = 0.33$ mm	$r_c = 0.44$ mm
$\rho_S = R_{400-440} / R_{500-560}$	1.27 ± 0.15	1.27 ± 0.14	1.34 ± 0.21
$\rho_L = R_{740-830} / R_{500-560}$	0.61 ± 0.12	0.62 ± 0.12	0.58 ± 0.11
Bundle areas	32	37	18

used to grade degrees of damage for those bundles selected for RNFL reflectance analysis.

Reflectance of RNFL Underlying Tissue in Normal and Glaucomatous Retinas

In the reflectance images of a normal retina, nerve fiber bundles appeared as bright stripes against a darker background (Fig. 1). Bundles were often separated by gaps between bundles. In this study, the reflectance of gaps was used to estimate the reflectance of the retinal tissue underlying the RNFL. For each selected bundle area, the mean reflectance of nearby gaps was calculated (Fig. 1). Figure 3 shows the average reflectance spectra of the gap areas that were defined for the bundles used in this study. Gap reflectance varied with wavelength. However, the spectra of gap reflectance in normal and treated retinas were similar. The reflectance of the gaps at any wavelength was not statistically different between the groups ($P > 0.5$).

RNFL Reflectance Spectrum in Normal Retina

RNFL reflectance is wavelength dependent. As shown in Figure 4B, bundle reflectance was high at short wavelengths and decreased with increasing wavelength. To compare RNFL reflectance spectra, each spectrum was normalized to its $R_{500-560}$. Figure 4B displays the normalized spectra along the same bundle with the bundle areas defined in Figure 4A. The spectra were similar along the bundle.

To quantitatively compare RNFL reflectance spectra, reflectance ratios were calculated for each spectrum. Table 1 summarizes reflectance ratios of the control retinas. Both ρ_S and ρ_L were not statistically different along the bundles ($P > 0.81$).

Changes of RNFL Reflectance Spectrum in Glaucomatous Retina

Figure 5 shows typical patterns of RNFL reflectance spectra in retinas with different degrees of cytoskeletal distortion. The bundles in Figure 5 were selected near the ONH. For the bundle with normal-looking cytoskeletons (Fig. 5A), the reflectance spectrum had a similar pattern as in the control; however, the slope of the reflectance spectrum in the short wavelength range (400–480 nm) was shallower than in the control. For the bundle with F-actin distortion (Fig. 5B), the reflectance spectrum was flatter in the short wavelength range compared with the control and Figure 5A. In the bundle with distortion of all cytoskeletal components (Fig. 5C), the entire spectrum flattened across all wavelengths. It is important to note, however, that bundles with distortion of all components were still visible in reflectance images and their reflectance was still directional (data not shown).

Changes in RNFL reflectance spectra were different along bundles in glaucomatous retinas. Figure 6 demonstrates the reflectance spectra at different areas along the same bundle, which had no apparent distortion of the cytoskeleton. For the peripheral bundle area (r_c), the spectrum was similar to the control with an apparent decline of reflectance as the short and long wavelengths increased. However, as the bundle area approached the ONH, the decline of reflectance with increasing wavelength became less steep. The entire spectrum gradually became flat from r_c to r_a. Such spectral change was often found in the bundles with normal-looking and slightly distorted cytoskeletons.

To quantitatively compare reflectance spectra of different groups, reflectance ratios at the short and long wavelengths (ρ_S and ρ_L) were calculated for each measured spectrum and ρ_S and ρ_L averages were summarized in Figure 7A. The values of ρ_S and ρ_L of the control, also listed in Table 1, are discussed above. For bundles with normal-looking cytoskeletons, ρ_S and ρ_L of the peripheral regions (r_b and r_c) were not statistically different than the control ($P > 0.2$); however, both ρ_S and ρ_L of the bundle regions near the ONH (r_a) were significantly different than that of the control with lower ρ_S ($P < 0.01$) and higher ρ_L ($P < 0.04$). For bundles with early and apparent cytoskeletal distortion, ρ_S and ρ_L were significantly changed at all radii compared with the control ($P < 0.004$ for ρ_S and $P < 0.02$ for ρ_L), except for ρ_L at r_b. The bar graph in Figure 7A shows overall changes of ρ_S and ρ_L with increasing cytostruc-

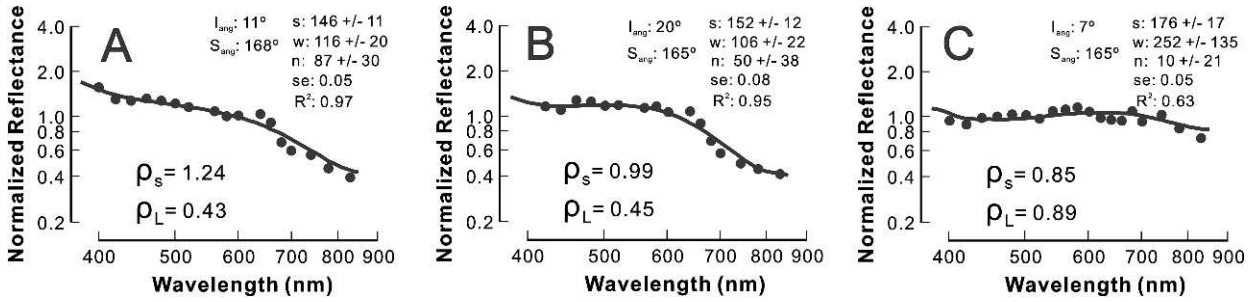

Figure 5. RNFL reflectance spectra of bundles with different degrees of cytoskeleton damage (bundle areas shown in Fig. 2). (**A**) Normal-looking cytoskeleton. The spectrum is similar to the control with slightly flat reflectance at short wavelengths. (**B**) Distorted F-actin. The spectrum has apparent change at short wavelengths. (**C**) Severely distorted cytoskeleton. The whole spectrum becomes flat. *Symbols*: measured reflectance. *Solid line*: fitted spectrum with a two-mechanism scattering model. I_{ang} and S_{ang}: incident and scattering angles, respectively. *s*, *w*, *n*: fitted parameters (see text for details). ρ_S and ρ_L: reflectance ratios calculated from measured data points. Reflectance spectra are normalized to the average reflectance at 500 to 560 nm and plotted on log-log coordinates.

tural damage—that is, ρ_S decreased with increased cytoskeletal damage while ρ_L gradually increased with increased axonal damage. For the bundles near the ONH, ρ_S of G2 and G3 decreased significantly compared with G1 ($P < 0.03$).

Two-Mechanism Model Fitting of RNFL Reflectance Spectrum

Change of RNFL reflectance indicates underlying structural change of axons. To evaluate relative contributions of different structural mechanisms to RNFL reflectance, measured reflectance spectra were fitted with a two-mechanism scattering model. Figure 7B summarizes the fitted parameters. In each of the normal retinas, *s*, *w*, and *n* were similar along bundles, which is consistent with the results by comparing ρ_S and ρ_L along the same bundles described above. In glaucomatous retinas, *s* of G1 and G2 was similar to the control but significantly increased in G3 at all radii ($P < 0.003$). Compared with the control, *w* was not statistically different at any treated groups and radii. For the bundles at r_a and r_b, the number of thin cylinders (*n*) was significantly decreased in all three groups ($P < 0.001$). For the bundles at r_c, *n* decreased significantly in G2 and G3 ($P = 0.05$ for G2 and $P = 0.006$ for G3) but not in G1 ($P = 0.12$), though *n* of G1 was lower than the control. Similarly, the bar graph in Figure 7B shows gradual decrease of *n* with increasing cytostructural damage.

Discussion

RNFL reflectance is often used in optical methods for RNFL assessment in the clinical diagnosis of glaucoma, yet little is known about the reflectance properties of RNFL under the development of glaucoma (Vermeer KA, et al. *IOVS* 2011;52:ARVO E-Abstract 3666).[27] This study provided comprehensive understanding of the changes in RNFL reflectance spectra that occur in a rat model of glaucoma. RNFL reflectance spectra were studied in normal retina and in nerve fiber bundles of treated retina with normal-looking appearance, early F-actin distortion, and apparent damage of the axonal cytoskeleton. Because glaucoma causes nonuniform damage of axons across the retina,[19,21,25,34–36] RNFL reflectance spectra were also studied at different radii from the ONH.

In normal retina, RNFL reflectance was high at visible wavelengths and declined with increasing wavelengths. Reflectance spectra of the normal RNFL were similar along bundles. Similarity of spectra along bundles suggests that the underlying structure contributing to RNFL reflectance does not change very much along bundles in normal retina.

Glaucomatous damage causes loss of RNFL reflectance (Vermeer KA, et al. *IOVS* 2011;52:ARVO E-Abstract 3666).[27,28] However, the reflectance of gaps did not change with the damage (Fig. 3), which suggests that glaucomatous damage does not significantly change the scattering structure of retinal layers other than the RNFL. This result is also consistent with no apparent morphological changes in outer retinal layers of glaucomatous retina reported by other groups.[29,37–39] For the reflectance of the RNFL only, our early study shows that glaucomatous damage causes decrease of RNFL reflectance, which occurs at all wavelengths and prior to RNFL thickness change.[27] The current study further showed that change of RNFL reflectance was wavelength dependent and reflectance at short wavelengths changed more than that at long wavelengths. The result indicates that changes of RNFL reflectance at short wavelength is more sensitive to damage at least in the early stages of glaucoma. The finding provides a possible explanation for the clinical observations that subtle RNFL defects can be identified by red-free fundus photography but not infrared OCT.[8–13]

Changes of RNFL reflectance spectra were found in bundles with different degrees of cytoskeletal damage. Among treated groups, decrease of ρ_S and increase of ρ_L became more evident with increases in cytostructural distortion (Figs. 5, 7A). In retinas with apparent cytostructural damage, the reflectance was approximately constant across wavelengths (Fig. 5C). These results suggest that RNFL reflectance change is correlated with the degree of cytostructural damage. However, exceptions to this pattern of spectral changes were also found in several bundles with a severely damaged cytoskeleton. In these bundles, the reflectance spectra were similar to the control. One interpretation is that the measured reflectance arises from the remaining normal axonal cytostructure. On the other hand, this study also found that changes of RNFL reflectance spectra occurred in bundles without apparent distortion of the cytoskeleton. One possible explanation is that cytostructural density decreases before detectable structural distortion. Because reflectance of the RNFL depends on the

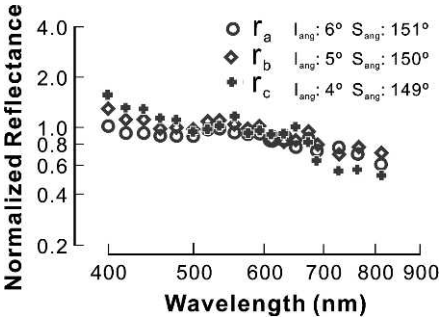

Figure 6. RNFL reflectance spectra along one bundle in a glaucomatous retina with normal-looking cytoskeleton. The spectra are different along the bundle. The slope of reflectance decrease at short wavelengths becomes shallower as the bundle area approaches the ONH. The whole spectrum looks flatter at r_a, while the spectrum at r_c is similar to that of normal. $r_a = 0.22$ mm, $r_b = 0.33$ mm, and $r_c = 0.44$ mm from the center of the ONH. Reflectance spectra are normalized to the average reflectance at 500 to 560 nm and plotted on log-log coordinates. I_{ang}, S_{ang}: incident and scattering angles.

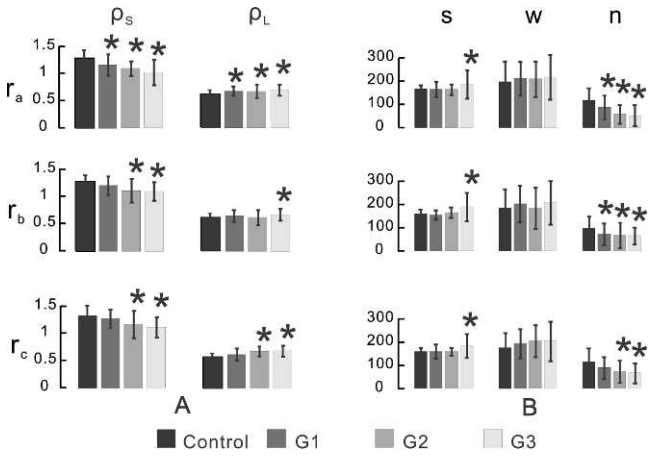

Figure 7. Quantitative comparisons of RNFL reflectance spectra. (**A**) Calculated reflectance ratios ρ_S and ρ_L. (**B**) Fitted parameters (*s*, *w*, *n*) of different groups at radii of 0.22 (r_a), 0.33 (r_b), and 0.44 (r_c) mm from the center of the ONH. *s* and *w* are measured in nanometers. *n* is the number of thin cylinders. *G1*: bundles with normal-looking cytoskeleton. *G2*: bundles with distorted F-actin. *G3*: bundles with severely distorted F-actin, MTs, and NFs. *Indicates statistically significant difference between the treated groups and the control.

relative refractive index of the tissue, another explanation could be that glaucomatous damage changes the optical properties of extracellular constituents before distorting axonal cytoskeleton.[40]

Although glaucoma causes distortion of the ultrastructure and change in the RNFL reflectance spectrum, the directional reflectance property of nerve fiber bundles was always present, which suggests that even in the damaged RNFL, cylindrical structures are the principal contributor to its reflectance. To study the relationship between changes of RNFL reflectance spectra and scattering structures contributing to RNFL reflectance, we used a two-mechanism scattering model to fit reflectance spectra. Because MTs are experimentally confirmed to contribute to RNFL reflectance, the radius and relative refractive index of MTs were used in the modeling of thin cylinders. However, thin cylinders can be any cylindrical structure with a radius much less than the shortest wavelength. The thick cylinders are not required to be circular, but must be oriented parallel to the nerve fiber bundles. Candidate structures could include mitochondria within axons, glial processes between axons, and/or even those cylindrical regions with a refractive index different than their surrounding medium, such as regional condensations of cytoskeleton or other constituents. In this study, the number of thin cylinders per unit-thick cylinder mechanism (n) was found to significantly decrease in all studied groups; while the average radius of thick cylinders increased in bundles with apparently damaged retinas (Fig. 7B). The decrease of n indicates a reduced contribution of scattering by thin relative to thick cylinder mechanisms. Because glaucoma damages axonal structures, it is plausible to speculate that the decrease of n represents the loss of thin cylinders, which is consistent with the decrease of RNFL birefringence, and hence the number of MTs, found in glaucomatous retinas.[16,41–44] The decrease of n was found on bundles with normal-looking cytostructures (G1 in Fig. 7B), which suggests that the loss of thin cylinders may occur early in the context of glaucoma, and that the RNFL reflectance at short wavelengths may be more sensitive to glaucomatous damage.

The increased radius of thick cylinders found in group G3 might be explained by increased glial tissue and abnormal accumulation of membrane-bound vesicles and mitochondria in glaucomatous retina,[45–48] but this study did not aim to associate RNFL spectral change with damage of specific cytoskeletal components and other retinal structures. Future studies should use more refined methods, such as electron microscopy, to investigate the anatomic basis for the cylinder mechanisms and provide quantitative correlation between changes of RNFL reflectance spectra and ultrastructure of retina.

Two striking features of the changes in RNFL reflectance spectra were found in this study: flattening of reflectance spectra was more evident in bundles near the ONH and spectral flattening even occurred in bundles without apparent structural distortion (Figs. 5A, 6). These results are consistent with the findings that the axonal cytostructure near the ONH is more sensitive to glaucomatous damage[24,25,49] and the RNFL reflectance decreases before thinning of RNFL (Vermeer KA, et al. *IOVS* 2011;52:ARVO E-Abstract 3666).[27,28] Together, these findings have a significant clinical implication in the diagnosis and management of glaucoma—that is, measuring RNFL reflectance near the ONH may provide detection of glaucomatous damage at a time during which damage of ganglion cell axons is reversible.

Although direct measurement of RNFL reflectance provides a more sensitive detection of RNFL damage than measuring RNFL thickness, it is difficult in practice to accurately measure absolute reflectance of the RNFL.[15,50] This study presented evidence that reduction of RNFL reflectance is not uniform across wavelength and reflectance ratios, as ρ_S and ρ_L used in this study significantly changed at an early stage of glaucoma. Recently developed dual-wavelength OCT demonstrates the feasibility of measuring the RNFL reflectance at 415 nm and 808 nm in rat retinas.[51] Simultaneous measurement of RNFL reflectance at different wavelengths may provide a new means for sensitive detection of early glaucomatous damage.

Acknowledgments

The authors thank Wei Shi for providing statistical analysis.

References

1. Hoyt WH, Frisen L, Newman NM. Fundoscopy of nerve fiber layer defects in glaucoma. *Invest Ophthalmol*. 1973;12:814–829.
2. Quigley H, Miller NR, George T. Clinical evaluation of nerve fiber layer atrophy as an indicator of glaucomatous optic nerve damage. *Arch Ophthalmol*. 1980;98:1564–1571.
3. Sommer A, Katz J, Quigley H, et al. Clinically detectable nerve fiber atrophy precedes the onset of glaucomatous field loss. *Arch Ophthalmol*. 1991;109:77–83.
4. Schuman JS, Hee MR, Arya AV, et al. Optical coherence tomography: a new tool for glaucoma diagnosis. *Curr Opin Ophthalmol*. 1995;6:89–95.
5. Schuman JS, Hee MR, Puliafito CA, et al. Quantification of nerve fiber layer thickness in normal and glaucomatous eyes using optical coherence tomography. *Arch Ophthalmol*. 1995; 113:586–596.
6. Zangwill LM, Williams J, Berry CC, Knauer S, Weinreb RN. A comparison of optical coherence tomography and retinal nerve fiber layer photography for detection of nerve fiber layer damage in glaucoma. *Ophthalmol*. 2000;107:1309–1315.
7. Kanamori A, Nakamura M, Escano M, Seya R, Maeda H, Negi A. Evaluation of the glaucomatous damage on retinal nerve fiber layer thickness measured by optical coherence tomography. *Am J Ophthalmol*. 2003;135:513–520.
8. Hwang J-M, Kim T-W, Park KH, Kim DM, Kim H. Correlation between topographic profiles of localized retinal nerve fiber layer defects as determined by optical coherence tomography and red-free fundus photography. *J Glaucoma*. 2006;15:223–228.
9. Teesalu P, Tuulonen A, Airaksinen PJ. Optical coherence tomography and localized defects of the retinal nerve fiber layer. *Acta Ophthalmol Scand*. 2000;78:49–52.
10. Kim T-W, Park U-C, Park KH, Kim DM. Ability of Stratus OCT to identify localized retinal nerve fiber layer defects in patients with normal standard automated perimetry results. *Invest Ophthalmol Vis Sci*. 2007;48:1635–1641.
11. Soliman MAE, van den Berg TJTP, Ismaeil A-AA, de Jong LAMS, de Smet MD. Retinal nerve fiber layer analysis: relationship between optical coherence tomography and red-free photography. *Am J Ophthalmol*. 2002;133:187–195.
12. Greaney MJ, Hoffman DC, Garway-Heath DF, Nakla M, Coleman AL, Caprioli J. Comparison of optic nerve imaging methods to distinguish normal eyes from those with glaucoma. *Invest Ophthalmol Vis Sci*. 2002;43:140–145.
13. Nukada M, Hangai M, Mori S, et al. Detection of localized retinal nerve fiber layer defects in glaucoma using enhanced spectral-domain optical coherence tomography. *Ophthalmol*. 2011;118:1038–1048.
14. Zhou Q, Knighton RW. Light scattering and form birefringence of parallel cylindrical arrays that represent cellular organelles of the retinal nerve fiber layer. *Appl Opt*. 1997;36:2273–2285.

15. Knighton RW, Huang X-R Directional and spectral reflectance of the rat retinal nerve fiber layer. *Invest Ophthalmol Vis Sci*. 1999;40:639–647.
16. Knighton RW, Huang X-R, Zhou Q. Microtubule contribution to the reflectance of the retinal nerve fiber layer. *Invest Ophthalmol Vis Sci*. 1998;39:189–193.
17. Huang X-R, Knighton RW, Cavuoto LN. Microtubule contribution to the reflectance of the retinal nerve fiber layer. *Invest Ophthalmol Vis Sci*. 2006;47:5363–5367.
18. Balaratnasingam C, Morgan WH, Bass L, Cringle SJ, Yu D-Y. Time-dependent effects of elevated intraocular pressure on optic nerve head axonal transport and cytoskeleton proteins. *Invest Ophthalmol Vis Sci*. 2008;49:986–999.
19. Filippopoulos T, Danias J, Chen B, Podos SM, Mittag TW. Topographic and morphologic analyses of retinal ganglion cell loss in old DBA/2NNia mice. *Invest Ophthalmol Vis Sci*. 2006; 47:1968–1974.
20. Buckingham BP, Inman DM, Lambert W, et al. Progressive ganglion cell degeneration precedes neuronal loss in a mouse model of glaucoma. *J Neurosci*. 2008;28:2735–2744.
21. Huang X-R, Knighton RW. Altered F-actin distribution in retinal nerve fiber layer of a rat model of glaucoma. *Exp Eye Res*. 2009;88:1107–1114.
22. Fu CT, Sretavan D. Laser-induced ocular hypertension in albino CD-1 mice. *Invest Ophthalmol Vis Sci*. 2010;51:980–990.
23. Baltan S, Inman DM, Danilov CA, Morrison RS, Calkins DJ, Horner PJ. Metabolic vulnerability disposes retinal ganglion cell axons to dysfunction in a model of glaucomatous degeneration. *J Neurosci*. 2010;5644–5652.
24. Chidlow G, Ebneter A, Wood J, Casson R. The optic nerve head is the site of axonal transport disruption, axonal cytoskeleton damage and putative axonal regeneration failure in a rat model of glaucoma. *Acta Neuropathol*. 2011;121:737–751.
25. Huang X-R, Kong W, Zhou Y, Gregori G. Distortion of axonal cytoskeleton: an early sign of glaucomatous damage. *Invest Ophthalmol Vis Sci*. 2011;52:2879–2888.
26. Fortune B, Burgoyne CF, Cull GA, Reynaud J, Wang L. Structural and functional abnormalities of retinal ganglion cells measured In vivo at the onset of optic nerve head surface change in experimental glaucoma. *Invest Ophthalmol Vis Sci*. 2012;53:3939–3950.
27. Huang X-R, Zhou Y, Kong W, Knighton RW. Reflectance decreases before thickness changes in the retinal nerve fiber layer in glaucomatous retinas. *Invest Ophthalmol Vis Sci*. 2011;52:6737–6742.
28. van der Schoot J, Vermeer KA, de Boer JF, Lemij HG. The effect of glaucoma on the optical attenuation coefficient of the retinal nerve fiber layer in spectral domain optical coherence tomography images. *Invest Ophthalmol Vis Sci*. 2012;53: 2424–2430.
29. Levkovitch-Verbin H, Quigley HA, Martin KRG, Valenta D, Baumrind LA, Pease ME. Translimbal laser photocoagulation to the trabecular meshwork as a model of glaucoma in rats. *Invest Ophthalmol Vis Sci*. 2002;43:402–410.
30. Knighton RW, Huang X-R Visible and near-infrared imaging of the nerve fiber layer of the isolated rat retina. *J Glaucoma*. 1999;8:31–37.
31. Huang X-R. *Polarization properties of the retinal nerve fiber layer investigated with multispectral imaging micropolarimetry.* Coral Gables, FL: University of Miami; 2000. Thesis.
32. Huang X-R, Knighton RW, Shestopalov V. Quantifying retinal nerve fiber layer thickness in whole-mounted retina. *Exp Eye Res*. 2006;83:1096–1101.
33. Teukolsky SA, Vetterling WT, Flannery BP. *Numerical Recipes in FORTRAN*. 2nd ed. Boston, MA: Cambridge University Press; 1992;576.
34. Quigley HA, Addicks EM. Regional differences in the structure of the lamina cribrosa and their relation to glaucomatous optic nerve damage. *Arch Ophthalmol*. 1981;99:137–143.
35. Quigley HA, Nickells RW, Kerrigan LA, Pease ME, Thibault DJ, Zack DJ. Retinal ganglion cell death in experimental glaucoma and after axotomy occurs by apoptosis. *Invest Ophthalmol Vis Sci*. 1995;36:774–786.
36. Howell GR, Libby RT, Jakobs TC, et al. Axons of retinal ganglion cells are insulted in the optic nerve early in DBA/2J glaucoma. *J Cell Bio*. 2007;179:1523–1537.
37. Kendell KR, Quigley HA, Kerrigan LA, Pease ME, Quigley EN. Primary open-angle glaucoma is not associated with photoreceptor loss. *Invest Ophthalmol Vis Sci*. 1995;36:200–205.
38. Yu S, Tanabe T, Yoshimura N. A rat model of glaucoma induced by episcleral vein ligation. *Exp Eye Res*. 2006;83:758–770.
39. Hare WA, Ton H, Ruiz G, Feldmann B, Wijono M, WoldeMussie E. Characterization of retinal injury using ERG measures obtained with both conventional and multifocal methods in chronic ocular hypertensive primates. *Invest Ophthalmol Vis Sci*. 2001;42:127–136.
40. Guo L, Moss SE, Alexander RA, Ali RR, Fitzke FW, Cordeiro MF. Retinal ganglion cell apoptosis in glaucoma is related to intraocular pressure and IOP-induced effects on extracellular matrix. *Invest Ophthalmol Vis Sci*. 2005;46:175–182.
41. Huang X-R, Knighton RW. Microtubules contribute to the birefringence of the retinal nerve fiber layer. *Invest Ophthalmol Vis Sci*. 2005;46:4588–4593.
42. Fortune B, Wang L, Cull G, Cioffi GA. Intravitreal colchicine causes decreased RNFL birefringence without altering RNFL thickness. *Invest Ophthalmol Vis Sci*. 2008;49:255–261.
43. Cense B, Chen TC, Park BH, Pierce MC, De Boer JF. Thickness and birefringence of healthy retinal nerve fiber layer tissue measured with polarization sensitive optical coherence tomography. *Invest Ophthalmol Vis Sci*. 2004;45:2606–2612.
44. Huang X-R, Bagga H, Greenfield DS, Knighton RW. Variation of peripapillary retinal nerve fiber layer birefringence in normal human subjects. *Invest Ophthalmol Vis Sci*. 2004;45:3073–3080.
45. Morrison JC, Moore CG, Deppmeier LMH, Gold BG, Meshul CK, Johnson EC. A rat model of chronic pressure-induced optic nerve damage. *Exp Eye Res*. 1997;64:85–96.
46. Kaufman PL. Nitric-oxide synthase and neurodegeneration/ neuroprotection. *Proc Natl Acad Sci*. 1999;96:9455–9456.
47. Tezel G, Chauhan BC, LeBlanc RP, Wax MB. Immunohistochemical assessment of the glial mitogen-activated protein kinase activation in glaucoma. *Invest Ophthalmol Vis Sci*. 2003;44:3025–3033.
48. Flammer J, Mozaffarieh M. What is the present pathogenetic concept of glaucomatous optic neuropathy? *Surv Ophthalmol*. 2007;52:S162–S173.
49. Balaratnasingam C, Morgan WH, Bass L, Matich G, Cringle SJ, Yu D. Axonal transport and cytoskeletal changes in the laminar regions after elevated intraocular pressure. *Invest Ophthalmol Vis Sci*. 2007;48:3632–3644.
50. Knighton RW, Baverez C, Bhattacharya A. The directional reflectance of the retinal nerve fiber layer of the toad. *Invest Ophthalmol Vis Sci*. 1992;33:2603–2611.
51. Zhang X, Hu J, Knighton RW, Huang X-R, Puliafito CA, Jiao S. Dual-band spectral-domain optical coherence tomography for in vivo imaging the spectral contrasts of the retinal nerve fiber layer. *Opt Exp*. 2011;19:19653–19659.